Title
A Method for Intertemporal Functional-Domain Connectivity Analysis: Application to Schizophrenia Reveals Distorted Directional Information Flow

Journal
IEEE Transactions on Biomedical Engineering, 63(12)

ISSN
0018-9294

Authors
Miller, Robyn L
Vergara, Victor Manuel
Keator, David B
et al.

Publication Date
2016-12-01

DOI
10.1109/tbme.2016.2600637

Peer reviewed

Published in final edited form as:

IEEE Trans Biomed Eng. 2016 December ; 63(12): 2525–2539. doi:10.1109/TBME.2016.2600637.

A Method for Inter-temporal Functional Domain Connectivity Analysis: Application to Schizophrenia Reveals Distorted Directional Information Flow

Robyn L. Miller,
Mind Research Network, Albuquerque, NM 87106 USA

Victor M. Vergara,
Mind Research Network, Albuquerque, NM 87106 USA

David B. Keator, and
Brain Imaging Center at the University of California-Irvine, Irvine, CA, 92697 USA

Vince D. Calhoun [Fellow, IEEE]
Department of Electrical and Computer Engineering, University of New Mexico and the Mind Research Network, Albuquerque, NM 87106, USA

Abstract

Objective—We introduce a method for analyzing dynamically changing fMRI brain network connectivity estimates as they vary within and between broad functional domains. The method captures evidence of intertemporal directionality in *cross joint functional domain* influence, and extends standard whole-brain dynamic network connectivity approaches into additional functionally meaningful dimensions by evaluating transition probabilities between clustered intra-domain and inter-domain connectivity patterns.

Results—In applying this method to a large (N=314) multisite resting-state fMRI dataset balanced between schizophrenia patients and healthy controls, we find evidence of joint functional domains that are *global catalyzers*, broadly shaping downstream functional relationships throughout the brain. Multiple interesting differences between patients and controls in both time-varying joint functional domain connectivity patterns and in cross joint functional domain intertemporal information flow were identified.

Conclusion and Significance—Our proposed approach thus unifies the concepts of brain connectivity and inter-domain connectivity and provides a powerful new way to evaluate functional connectivity data in the context of both the healthy and diseased brain.

Index Terms

Brain imaging; brain networks; fMRI; dynamic connectivity; functional connectivity; schizophrenia

Correspondence to: Robyn L. Miller.

I. Introduction

While interest in dynamically varying properties of resting state brain connectivity has grown considerably in recent years [1, 2], the tools applied in these studies still limit the scope and power of potential findings. To be sure, there are various conceptual approaches to connectivity within the functional imaging community, each with strengths and weaknesses. Among these are very detailed, highly-parametrized, nonlinear regional models that tend to assume the same response to each stimulus and are applied to only a few regions at a time due to the parametric burden [3, 4], linear models of lagged nodal or voxelwise relationships [5] and a very extensive literature in whole-brain functional network (or region-of-interest (ROI)) connectivity, typically based on covariance between the timecourses of spatially distributed networks (or ROIs) that cover all voxels in the brain [6]. Our proposed framework extends and reconceives the dynamic variants of this latter approach that are based on clustered time-varying measures of functional network connectivity computed over sliding windows through network timecourses [7–9]. The existing sliding-window whole-brain functional-network connectivity (WinFNC) approaches have several limitations that our framework mitigates: (1) WinFNC approaches yield very low-dimensional representations of intricate dynamics. Although often operating on the whole-brain level, computing 1000+ dimensional FNC matrices for each window, the *dynamic dimension*, i.e., the dimension of the state space, in these analyses is typically very low, not infrequently as low as 1-dimension. (2) WinFNC approaches ignore the temporal directionality of network interactions. Based on covariance, the window-wise computed FNC matrices are indeed symmetric, but the fact that they are computed on many time windows can be leveraged to obtain notions of directional influence that have to date been underexpelored. (3) WinFNC approaches have focused on the whole the whole brain, yielding limited insight into specialized dynamical behavior within and between particular functional domains. In this paper we introduce a straightforward intuitive approach to analyzing *dynamic directional functional domain connectivity* (ddFDC). This method extends and refines the WinFNC approach, operating at a dimensional scale sufficient to capture multiplexed dynamical relationships within and between functional domains and capturing directional intertemporal influence between functional domains. In an application to resting fMRI data from a large balanced schizophrenia study, we find that relationships involving cognitive control (CC) networks, subcortical (SC) networks, and the default mode networks (DMN) play unusually large roles in shaping subsequent functional behavior throughout the brain. We also find significant differences in directional functional information flow between controls (HC) and schizophrenia patients (SZ), as well as distinct directional asymmetries among patients.

II. Methods

Our method builds on the common sliding-window approach to studying dynamic brain network connectivity [7, 8]. Functional MRI data are preprocessed and, using group ICA (GICA) [9], decomposed into a set of functionally meaningful, temporally coherent distributed networks that are maximally spatially independent. Subject-specific network timecourses (TCs) are also produced. Using a sliding-window though the network TCs, time-varying snapshots of whole-brain functional network connectivity (FNC) are produced by computing the pairwise correlations between networks on successive windows. Suppose

there are N subjects, T windows and M networks. This yields an ordered set of T windowed FNCs (wFNCs) for each subject. The networks whose time-varying relationships are captured in the wFNCs can be grouped into broad functional categories, or *functional domains* (*FDs*) (Fig. 1).

Assume there are D functional domains. Typically, this grouping is done before the FNCs are computed to allow for more visually interpretable FNC images, in which networks are organized by domain along the axes of the matrix image (Fig. 2). Organized in this way, FNCs become a disjoint union of D^2 rectangles (of which only $\frac{D(D+1)}{2}$ are distinct, due to symmetry of the FNC matrix) that feature the connections between networks in a specific pair of FDs, or *joint functional domains* (*JFDs*). These specialized domain-to-domain patterns of connectivity (*JFDCs*), are the main focus of our work. We are interested in the time-varying windowed connectivity (*wJFDCs*) between networks in each JFD, and more specifically in the intertemporal influence of JFDCs upon each other.

To probe these questions, we separately cluster the NT observed wJFDCs associated with each JFD. This produces a (study-wide) collection of D sets of cluster centroids, and D corresponding length-T JFDC cluster-occupancy timeseries for each subject. At each timestep, each subject occupies exactly one cluster in each of the D JFDCs. The fundamental question of interest is whether the time t network connectivity structure within certain JFDs present evidence of informing the time $t + \Delta t$ connectivity structure within other JFDs. To this end, for each subject in the study we induce a complete weighted directed graph between pairs of JFDs based on the degree to which cluster occupancies in a target JFDC are conditioned upon cluster occupancies in a source JFDC at the immediately preceding timestep. The dimension of the FNC the source and target JFDCs are usually different, but one strength of our method is that it captures pairwise intertemporal directional information flow between data sources and targets of arbitrary dimension. The functional form of the measured relationships is also unconstrained, and certainly need not be linear as is so often assumed in functional connectivity studies (Fig. 3).

A. Study Participants and Early Data Processing

1) Subjects and Imaging Parameters—Our fMRI data comes from a large (N=314; 231 male (M), 83 female (F)) multisite study, balanced between schizophrenia patients (151 SZ) and healthy controls (163 HC) [9]. The subjects were instructed to keep their eyes closed during the scan and were not engaged in any specified task. The ages of participants ranged between 18 and 60 (mean 37.9). Informed consent was obtained from all subjects according to the institutional guidelines the seven participating data collection sites. Imaging from six of the sites was performed on a 3T Siemens Trio scanner; the seventh site used a 3T GE MR750. A total of 162 volumes of resting fMRI data was acquired for each subject using a gradient-echo planar imaging paradigm: FOV of 220×220 mm (64×64 matrix), TR=2 s TE = 30 ms, flip angle = 77°, slice thickness = 4 mm, slice gap = 1 mm, voxel size = 3 mm^3. A combination of toolboxes (AFNI1, SPM2, GIFT3) and custom code written in Matlab was employed in the pre-processing pipeline. Rigid body motion correction was performed with the INRIAlign toolbox in SPM to correct for subject head motion, followed

by slice-timing correction to account for timing differences in slice acquisition. Additional details can be found in [9].

2) Group ICA and Time-Varying Network Connectivity—Group ICA (http://mialab.mrn.org/software/gift) was applied to all subjects' fMRI data with initial model order 100, from which 47 components were eventually identified as meaningful resting state networks (RSNs) [9, 10]. Subject-specific spatial maps and time courses were obtained using spatio-temporal regression. The subject RSN time courses were detrended, orthogonalized with respect to motion parameters, despiked by replacing outlier time points with 3rd order spline fit to cleaner neighboring points, and filtered using a 5th order Butterworth filter with a passband of 0.01 to 0.15 Hz.

3) Windowed Functional Connectivity Matrices—Whole brain windowed functional network connectivity (wFNC) was evaluated by computing pairwise correlations between all 47 RSNs on windowed segments of network timecourses using a tapered rectangular window of length of 22 TRs (44 seconds), advancing 1 TR at each step. To improve correlation estimates on timecourses of shorter length, we impose an L^1 constraint on the inverse covariance matrix using the G-LASSO framework, with regularization parameter optimized subject-wise by evaluating the log-likelihood of each subject's unseen data in a cross-validation framework, yielding 136 47×47 windowed functional network connectivity matrices (wFNCs) for each subject [9].

B. Joint Functional Domains (JFDs) and Windowed Joint Functional Domain Connectivity (wJFDC)

The 47 identified RSNs were initially organized into seven broad *functional domains* (*FDs*) [9], which we further consolidated into five: auditory-visual-sensorimotor networks (AVSN), cognitive control (CC), cerebellar (CR), default mode network (DMN) and subcortical (SC). Networks are arranged along axes of each wFNC matrix image according to domain membership, allowing wFNCs to be decomposed into a disjoint union of 25 rectanglular blocks determined by domain boundaries (Fig. 4) along each axis.

The domain-pairs bounding these rectangles are called *joint functional domains* (*JFDs*), and the rectangular blocks of the wFNC corresponding to any particular JFD are called *JFDCs* (or *wJFDCs* in the windowed case). They consist only of connectivity measures between networks in the bounding FDs. Since the wFNCs are symmetric, only 15 of the 25 JFDCs contain distinct data (Fig. 4).

C. Clustering of wJFDCs and JFD-Specific Dynamic Connectivity States

At a study-wide level there are $NT = (314)(136) = 42{,}704$ observations of each of the $D = 15$ JFDCs (N = #of subjects, T = #of windows). Kmeans clustering (squared Euclidean distance, 500 replicates, 1500 iterates, number of clusters chosen with the silhouette criterion) was applied separately to the 42,704 observations of each JFDC, producing 15 sets of JFDC-specific cluster centroids and occupancy measurements (Fig. 5). Every subject has 15 length-136 cluster occupancy timeseries, the d^{th} of which contains elements in $\{1,2,..,n_d\}$, where n_d = #of clusters in the d^{th} JFDC, $d = 1,2, \ldots,15$. In the current study, $n_d \in$

{2,..,7}. This yields 15 sets of cluster occupancy rates $\left\{\left\{\tilde{P}_c^{(d)}\right\}_{c=1}^{n_d}\right\}_{d=1}^{15}$ for each subject. The vector of cluster occupancy rates in each domain always sums to 1 for each subject. The JFDC clusters always contain many observations. However, since clustering was done at a study-wide level not every subject visits every cluster of every JFDC, ie some occupancy rates are zero. The number of clusters that a subject occupies at least once in the d^{th} JFDC is denoted by n_d^*; the associated non-zero vectors of cluster occupancy rates for each JFDC are given as $\left\{\left\{\tilde{P}_c^{(d)^*}\right\}_{c=1}^{n_d^*}\right\}_{d=1}^{15}$.

D. Conditional Probabilities Between JFDCs

For each subject and each ordered pair F_i, F_j of JFDCs $i, j \in \{1,2,\ldots,15\}$, we compute

$$P_{i,j}=\left(p_{r,c}^{(i,j)}\right)_{r,c=1}^{n_i,n_j}$$

the probabilities

$$P_{r,c}^{(i,j)}=p\left(C_c^{(j)}(t+1)|C_r^{(i)}(t)\right)$$

of that subject being in the c^{th}, $c \in \{1,..,n_j\}$ cluster of F_j at time $t+1$ *conditional on* the subject having been in the r^{th}, $r \in \{1,..,n_i\}$ cluster of F_i $(i \neq j)$ at time t. These conditional probability matrices, referred to as *transition probabilities*, row-sum to one and act like Markov transition matrices between JFDC cluster structures (Fig. 6, Fig. 7).

E. Information Flow Between JFDCs

We consider a source JFDC F_i to be *informative* about a target JFDC F_j if the probabilities of occupying clusters in the target at time $t+1$ depend heavily on which cluster in the source JFDC at time t is being conditioned upon. There are two criteria we require for the metric $\mathscr{J}_{i,j}$ of intertemporal information flow from F_i to F_j: (i) it should increase in how dissimilar the full distribution over target clusters from different originating source clusters, and (ii) should also increase in how well clusters of the target separate over clusters of the source. To this end, we introduce two informational measures, each tuned to one of the objectives: $\mathscr{D}_{i,j} \in [0,1]$ for the degree of broad distributional dissimilarity and $\mathscr{S}_{i,j} \in [0,1]$ for the degree to which source clusters map preferentially to some specific target cluster. The overall information metric $\mathscr{J}_{i,j} \in [0,1]$ is the average of $\mathscr{D}_{i,j}$ and $\mathscr{S}_{i,j}$ (Fig. 3, Fig. 8).

Although cluster occupancy rates are of significant stand-alone interest, non-occupied source clusters (resp. target clusters) do not distribute over target clusters (resp. are not distributed over by source clusters) and do not map preferentially to target clusters (resp. are not mapped preferentially into by source clusters) and thus are not relevant inputs to the *cross-JFDC* (*xJFDC*) information metric. Instead, when there are non-occupied clusters in source or target JFDCs we use a reduced probability matrix

$$P^*_{i,j}=\left(p^{(i,j)}_{r,c}\right)^{n^*_i,n^*_j}_{r,c=1}$$

as input to the xJFDC information computations, where $n^*_i \leq n_i$ and $n^*_j \leq n_j$ are the number of source and target clusters the subject has occupied at least once. The L^2 distances between rows of $P^*_{i,j}$ capture (pairwise) distributional dissimilarity of source clusters over target clusters. Since rows of $P^*_{i,j}$ sum to 1, the L^2 distances between them are bounded in $[0,\sqrt{2}]$. When $n^*_i \leq n^*_j$ we simply average the distances between different rows of $P^*_{i,j}$ and rescale by $1/\sqrt{2}$ to obtain a quantity in [0,1]:

$$\mathscr{D}_{i,j}=\frac{v_{i,j}}{\sqrt{2}}\frac{2}{n^*_i(n^*_i-1)}\sum_{\substack{r'>r\\ \in\{1,..,n^*_i\}}}\sqrt{\sum_{c=1}^{n^*_j}(p^*_{r,c}-p^*_{r',c})^2}$$

$$v_{i,j}=\begin{cases}1, & n^*_i \leq n^*_j\\ \psi^{-1} & n^*_i>n^*_j\end{cases}$$

where

$$\psi=1-2\frac{\left(\left(n^*_j(1+m)-n^*_j\right)\binom{m}{2}+\left(n^*_i-n^*_j m\right)\binom{M}{2}\right)}{n^*_i(n^*_i-1)}<1$$

$m=\left\lfloor n^*_i/n^*_j\right\rfloor$, $M=\lceil n^*_i/n^*_j\rceil$ is the maximum achievable value of $D_{i,j}=\frac{1}{\sqrt{2}}\frac{2}{n^*_i(n^*_i-1)}\sum_{\substack{r'>r\\ \in\{1,..,n^*_i\}}}\sqrt{\sum_{c=1}^{n^*_j}\left(p^*_{r,c}-p^*_{r',c}\right)^2}$ for probability transition matrices with n^*_i rows and n^*_j columns. The minimum $\mathscr{D}_{i,j}=0$ occurs when the distribution over clusters in F_j is independent of the cluster occupancies in F_i at the preceding timestep. And, subject to application of the matrix size correction factor $v_{i,j}$, the metric peaks at $\mathscr{D}_{i,j}=1$ when clusters of F_j perfectly separate over clusters of F_i. Note that away from the extreme upper and lower bounds of $\mathscr{D}_{i,j}$ one can readily find cases in which the full distributions of different source clusters over target clusters are pointwise quite dissimilar, even when none of the source clusters map with extremely high probability to specific target clusters. Conversely, distinct source clusters with very pointwise similar full distributions over the target clusters can each strongly separate the target clusters (for example $P^*_{i,j}=\begin{pmatrix}0 & 1\\ 0.1 & 0.9\end{pmatrix}$. A fair assessment of cluster-level source-target preferential mapping specificity requires balanced consideration of both the raw maximum values along each row of $P^*_{i,j}$ and the magnitude of these row-maxima *relative* to population-level (non-conditional)

target cluster occupancy probabilities $\left\{\tilde{P}_k^{(j)^*}\right\}_{k=1}^{n_j^*}$ of occupied, ie $\tilde{P}_k^{(j)}>0$, clusters in F_j. The specificity metric, $\mathscr{S}_{i,j}\in[0,1]$, we employ represents a balance of these considerations:

$$\mathscr{S}_{i,j}=\frac{1}{n_i^*}\sum_{r=1}^{n_i^*}\max_{c\in\left\{1,..,n_j^*\right\}}\left\{\zeta_{r,c}^{(i,j)}\right\}$$

where

$$\zeta_{r,c}^{(i,j)}=\frac{p_{r,c}^*-\tilde{P}_c^{(j)^*}}{1-\tilde{P}_c^{(j)^*}}\leq 1$$

is negative when $p_{r,c}^*<\tilde{P}_c^{(j)^*}$ and otherwise represents the proportion of the interval between the population-wide cluster occupancy probability, $\tilde{P}_c^{(j)^*}$, and 1 that is filled by $[\tilde{P}_c^{(j)^*}, p_{r,c}^*]$. Thus, $\zeta_{r,c}^{(i,j)}$ is identically 1 when $p_{r,c}^*=1$ identically 0 when $p_{r,c}^*=\tilde{P}_c^{(j)^*}$ and otherwise $\zeta_{r,c}^{(i,j)}$ approaches 1 linearly in $p_{r,c}^*$ with slope, $\frac{1}{1-\tilde{P}_c^{(j)^*}}$, dependent on $\tilde{P}_c^{(j)^*}$. A large value of $\mathscr{S}_{i,j}$ indicates that the average source cluster maps very preferentially to a target cluster, with linear correction for the overall occupancy rate of the target cluster.

Finally, we take $\mathscr{J}_{i,j}$ to be a convex combination, in our case the mean of $\mathscr{D}_{i,j}$ and $\mathscr{S}_{i,j}$:

$$\mathscr{J}_{i,j}=\lambda_1\mathscr{D}_{i,j}+\lambda_2\mathscr{S}_{i,j},\quad \lambda_1-\lambda_2=0.5$$

Although clearly $P_{i,j}^*=P_{k,l}^*\Rightarrow\mathscr{J}_{i,j}=\mathscr{J}_{k,l}$, there are many very different ways to produce the same level of information flow from one JFDC to another, i.e., $\mathscr{J}_{i,j}=\mathscr{J}_{k,l}\not\Rightarrow P_{i,j}^*=P_{k,l}^*$. for example, if $P_{i,j}^*\begin{pmatrix}1&0\\0&1\end{pmatrix}$ and $P_{k,l}^*\begin{pmatrix}0&1\\1&0\end{pmatrix}$, the transition probabilities are completely different and yet $\mathscr{J}_{i,j}=\mathscr{J}_{k,l}=1$. The metric is a high-level summary of the degree to which a target JFDC at time $t+1$ is conditioned upon a source at time t without regard to *how* this conditioning manifests at the more granular level of cluster-to-cluster transition probabilities.

F. Cross-JFDC Information Flow Asymmetry

The metric $\mathscr{J}_{i,j}$ of cross-JFDC intertemporal information flow is not symmetric in the JFDCs: $\mathscr{J}_{i,j}\neq\mathscr{J}_{j,l}$. The signed informational asymmetry between JFDC F_i and JFDC F_j is defined as $\mathscr{J}_{i,j}^{\perp}=\mathscr{J}_{i,j}-\mathscr{J}_{j,i}$. The absolute informational asymmetry is $\mathscr{J}_{i,j}^{|\perp|}=|\mathscr{J}_{i,j}-\mathscr{J}_{j,i}|$.

G. Intra-JFDC Dynamism

One concrete situation that can lead to zero intertemporal xJFDC information flow is the "degenerate occupancy condition" in which a subject occupies only one cluster in either the target or the source JFDC. Although degenerate occupancy leads to identically zero information flow, near-stasis in one or both JFDCs, i.e., when a subject spends very long contiguous stretches of time in particular source or target JFDC clusters can also constrain xJFDC information flow. Negligible xJFDC information flow resulting from subject stasis in the source and/or target JFDC is an important phenomenon in its own right. Having a rough summary measure of *intra-JFDC dynamism* however can provide useful context for interpreting intertemporal xJFDC information flow. The intra-JFDC dynamism measure d_i for JFD F_i is computed from the square intertemporal F_i-to-F_i transition probability matrix $P_{i,i}=\left(p_{r,c}^{(i,i)}\right)_{r,c=1}^{n_i,n_i}$, $p_{r,c}^{(i,i)}=p\left(C_c^{(i)}(t+1)|C_r^{(i)}(t)\right)$ as the sum of the off-diagonal elements, rescaled by $1/n_i$:

$$d_i=\frac{1}{n_i}\sum_{c\neq r}p_{r,c}^{(i.i)}$$

Since all rows of $P_{i,i}$ sum to one, the maximal possible value for $\sum_{c\neq r}p_{r,c}^{(i,i)}$ is n_i, and rescaling by $1/n_i$ ensures that $d_i\in[01]$. Diagonal elements of $P_{i,i}$ contain probabilities that the subject has not changed cluster from time t to time $t+1$. Off-diagonal elements contain the probabilities of switching from one cluster at time t to a *different* cluster at time $t+1$, which is a good proxy for the subject's temporal dynamism (lack of stasis) in JFDC F_i.

H. Null Model for Significance

We computed a null distribution for $\mathscr{J}_{i,j}$ by simulating 10,000 pairs of length $T=136$ JFDC cluster occupancy timeseries, each with occupancies generated according to the cluster occupancy probabilities exhibited by two randomly chosen JFDCs from our data. The median of the resulting null distribution was $\mathscr{J}=0.14$; the 95$^{\text{th}}$ percentile significance cutoff was $\mathscr{J}=0.22$ and 99$^{\text{th}}$ percentile cutoff was and $\mathscr{J}=0.28$. The percentile cutoffs decay in T, with median = 0.11 for $T=200$, median = 0.08 for $T=400$ and median=0.06 for $T=800$.

I. Diagnosis Effects

Our diagnosis effects are derived from a linear regression model that includes age and gender as nuisance covariates. The diagnosis variable is binary with schizophrenia patients coded as '1' and controls as '0', so $\beta_{diagnosis}<0$ represents a negative correlation with SZ. We generally report or display the value of $\beta_{diagnosis}$ only when its false discovery rate (FDR) corrected p-value is less than 0.05.

J. Concise Methods Summary

In addition to standard pre-processing and network decomposition, the framework we have proposed requires several additional processing steps and also produces multiple outputs of interest. We are therefore provide a concise summary of the chain of methods detailed

above. In short, our framework separates domain-level blocks of time-varying FNC matrices and identifies, for each, a set of recurrent domain-level "dynamic states" through clustering. This enables us to study several measures of domain-scale functional connectivity dynamics. First, there is basic cluster occupancy rate information split out over the dynamic states associated with different pairs of functional domains (Sections II.B and II.C). We also can assess the degree of domain-level connectivity dynamism or dynamic variability (Section II.G). Most centrally, the method produces evidence that connectivity between networks in certain domains is dynamically shaped by connectivity between networks in other domains (Section II.E). Finally, the method allows us to assess the degree of symmetry evident in this shaping role of domain pairs upon each other (Section II.F).

III. Results

A. Dynamic Occupancy of wJFDC Clusters

The fifteen JFDCs ranged in dimensionality from 2 (CR-CR) to 247 (AVSN-CC), and the 42,704 windowed observations of each JFDC split into clusters numbering between 2 (AVSN-AVSN and CR-CR) and 7 (CC-DMN). The average subject realized 81% of the available clusters from each JFDC (Table 1). Our findings regarding schizophrenia and JFDC cluster occupancy are consistent with observations at the lower-dimensional whole-brain level [9, 11–17]. The multiplexing of whole-brain FNCs into multiple JFDCs, however, allows identification of more specialized recurring functional relationships that are relatively blurred out in whole-brain wFNCs Schizophrenia has broad and significant effects on JFDC cluster occupancy (Fig. 9). Whole-brain static and time-varying FNC findings of reduced connectivity [9, 12, 18, 19] in schizophrenia are evident at the JFDC level: among the clusters that have significantly elevated occupancy levels in schizophrenics are those with relatively low magnitude inter-network connectivity (i.e., Cluster 2 of AVSN-AVSN, Cluster 1 of AVSN-DMN, Cluster 5 of CC-SC from Fig. 9). Higher-level findings of generally reduced connectivity dynamism [14, 17] in schizophrenia at the whole-brain scale are also echoed in JFDCs: the number of clusters visited at least once is lower in schizophrenia patients for six of fifteen JFDCs (Table 1). The intra-JFDC intertemporal dynamism measure is also lower in most JFDCs, significantly so for AVSN-AVSN, AVSN-CR, ACSN-CC and CC-SC (Fig. 10).

B. Cross-JFDC Information Flow

Cross-JFDC information flow between most pairs of JFDCs is significant relative to a null hypothesis of independence (Fig. 11). This degree of interdependence is unsurprising for measurements taken on a functionally interconnected brain in which much activation is at least somewhat temporally conditioned on other functional connections on the t, $t + 1\,TR$ ($1\,TR$ = 2sec) timescale. Directional patterns in $\mathscr{J}_{i,j}$ means (Fig. 11) indicate that while some JFDCs (CC-DMN, CC-CC, SC-SC, CC-SC, AVSN-DMN) broadly influence subsequent functional connections throughout the brain. We will call this class of JFDCs *global catalyzers*. In terms of sensitivity to input, most JFDCs are dominantly tuned to the global catalyzers. There are some exceptions, for example CC-DMN is quite influenced by within-DMN connectivity (DMN-DMN), a JFDC which is not a global catalyzer. Tracing this influence forward, we can see DMN-DMN acts as a second-order catalyzer by strongly

influencing CC-DMN, the strongest of the global catalyzers. Although not a focus of this paper, the second-order influence of intra-DMN connectivity highlights the potential for fruitful application of directed graph theory on xJFDC information measures.

C. Cross-JFDC Information Flow Asymmetry

Relatively non-influential JFDCs can either be sensitive to input from the rest of the brain (AVSN-SC, CC-CR and CR-CR), i.e., merely *shy*, or truly *insular* (AVSN-AVSN), exhibiting limited sensitivity to other JFDCs as well as absence of influence. Although there tends to be strong intra-domain coordination among auditory-visual-sensorimotor networks (Fig. 4, Fig. 9), the particular form this within-domain connectivity takes has very limited impact on wider functional relationships in the brain – including JFDCs that in which AVSNs are a constituent FD, at least under eyes-closed, resting conditions. Although at the full population level, AVSN-AVSN is a relatively insular JFDC, there is evident directional asymmetry: AVSN-AVSN connectivity conditions somewhat less weakly on input from other JFDCs than the other way around. This asymmetry is even more pronounced for intra-cerebellar connectivity (CR-CR) which is of almost no interest to other parts of the brain but quite responsive to input (Fig. 11).

D. Cross-JFDC Information Flow: Schizophrenia Effects

The most significant effects of schizophrenia on xJFDC intertemporal information (Fig. 12, bottom row) flow are negative, and focused in the AVSN-AVSN, AVSN-CC, AVSN-CR, and CC-SC. Significant ($\alpha < 0.05$, without correction for multiple comparisons) negative effects of SZ also apply to AVSN-SC, SC-CR, SC-SC and DMN-DMN. This is consistent with results from static and dynamic FNC pointing to diminished connectivity in SZ [9, 12, 18–20], but addresses a higher “supra-network” level of information flow dysfunction that also has directional elements. The sensitivity of intra-AVSN connectivity to inputs from broader brain connectivity patterns is much higher in healthy individuals (Fig. 12, top row). So much so that AVSN-AVSN is a non-insular JFDC in the healthy population. The influence of intra-AVSN connectivity on the connectivity of other JFDCs is also higher in controls, though very limited relative to other JFDCs in both patients and controls.

In both populations the information inflow from other JFDCs into AVSN-AVSN is highly variable (Fig. 13, top row), and there is a general trend, consistent with recent results in the area of network spatial maps [21], of higher variability in xJFDC information flow among patients (Fig. 13, bottom row).

As is visually evident in figures (Fig. 11, Fig. 12) displaying $\mathscr{J}_{i,j}$, direct computation of cross-JFDC information asymmetry points to asymmetry strongly favoring information inflow for AVSN-AVSN and CR-CR in both patients and controls (Fig. 14, top row). The magnitude of the AVSN-AVSN directional information flow asymmetries are, however, significantly reduced in schizophrenia patients (Fig. 14, bottom right).

IV. Discussion

We have introduced a novel approach to study intertemporally directed information flow within and between broad functional brain domains using probability transition matrices

between separately clustered time-varying estimates of inter-domain and intra-domain connectivity. The framework yields various measures of interest, including the cluster centroids for each joint functional domain and the occupancy rates, a within-joint domain dynamism measure d_i evaluated on $P_{i,i}$, the high-level non-symmetric cross-JFDC information metric $\mathscr{J}_{i,j}$, and measures of signed $\mathscr{J}_{i,j}^{\perp}$ and absolute $\mathscr{J}_{i,j}^{|\perp|}$ information flow directional asymmetry. There are also the more granular cluster-level transition probabilities $p_{r,c}^{(i,j)}$ in each $P_{i,j}$ which were not reported upon here, but are themselves objects of interest that displayed significant group differences (patient vs. control) in our subject pool.

We applied the new framework to a large multisite resting fMRI study which was balanced between schizophrenia patients and controls, finding highly significant patient/control differences in all measures, generally indicative of reduced information flow, reduced dynamism, and attenuated intra-JFD connectivity. The general reduction among patients for measures related to connectivity strength and dynamism is consistent with results from other studies, and the reduced intra-JFD connectivity and cross-JFDC information flow can be viewed as a higher-level analogue of earlier findings, yet another layer of evidence for pervasive suppression of potentially informative brain activation among schizophrenia patients. We also identified several JFDs shared by both patients and controls, referred to as *global catalyzers*, that play an outsized role in shaping subsequent functional relationships throughout the brain. *Shy* or *insular* JFDCs, relatively cut off from the chain of cross-JFDC influence in one or both directions, were identified as well, although this characteristic was not always stable between patients and controls. Global catalyzers (CC-CC), shy (AVSN-AVSN, for healthy) and insular (AVSN-AVSN for patients) JFDCs, however, feature strongly among those whose xJFDC information flow is significantly affected by schizophrenia.

These findings provide compelling evidence that schizophrenia not only disrupts connectivity at the individual network level, but also significantly distorts directional patterns of organizational influence at the broader domain-scale of functional integration. A better understanding of healthy information flow and directional influence roles at this wider scale is particularly important as it could help clarify the levels at which other variables such as cognition and symptoms are more reflective of the disease, and help decouple some of the challenges highlighted in the recent research domain criteria (RDoC) initiative of the National Institutes of Health [22]. For example, although undirected network-level static and dynamic connectivity analyses have not yet yielded biomarkers for specific categories of hallucinatory experience (auditory, visual, somatosensory), by tuning domain and network resolution (network resolution can be refined or coarsened by adjusting the ICA model order), directional domain-scale information flows seem promising candidates for capturing distortions – possibly only evident directionally or at the scale of whole domains – that are strongly associated with particular psychotic symptomology. We are in fact intending to probe this possibility in the near future, initially by disaggregating the auditory, visual and sensorimotor domains but also by developing methods of tuning network and domain scaling in ways that optimize the analytic power of a method that deals with network aggregates in directional ways.

Although promising, there are of course some limitations to the framework as presently implemented. As with any high-level method, ours is only as good as its inputs; all the usual caveats apply in regard to preprocessing, network-extraction, window-length and the validity of correlation as a metric of network connectivity. The method however, is also distinctively sensitive to the initial assignment of networks to functional domains and to choices made at the clustering stage. The value and scope of the method would be enhanced by extensions such as those enumerated above, and also by further refinements of both the null model and the information metric.

In addition to opening up a new line of investigation in brain imaging data as proposed, there are a number of areas within the scope of the method itself that we are actively working on or have slated for future work. These areas include, but are not limited to:

1. *Nonstationarity*. Although the inputs to this method are windowed connectivity estimates, in this work we use all available measurements to compute the transition probabilities $P_{i,j}$. Certainly there is no a priori reason to believe that the $P_{i,j}$'s themselves are stationary, and a dynamical version of this analysis in which $P_{i,j}(w)$'s are computed separately on sliding windows through the windowed JFDC observations seems likely to yield novel insights.

2. *Memory Length and Breadth*. In this paper we assume that the dependency relations between two JFDCs, F_i and F_j, are Markovian: the probability of being in cluster c of JFDC F_j at time $t + 1$ conditional on behavior of F_i requires only knowledge of the cluster occupied in F_i at time t. Probing this assumption, developing ways to determine the optimal breadth and duration of memory (appropriate computation of occupancy probabilities in F_j conditional on F_i might require going further back than $t - 1$, and considering other JFDCs in addition to F_i as part of the memory process) and then building longer/broader probabilistic memory into the method would constitute an important extension of the current framework

3. *Directed Graph Theory*. As pointed out briefly in III.B, the matrix $\mathscr{J} = (\mathscr{J}_{i,j})$ can be viewed as a complete weighted directed graph $\mathscr{G}$ with nodes labeled by JFDCs. Since intertemporal directionality is embedded in the $\mathscr{G}$'s structure, any network or graph metrics computed on $\mathscr{G}$ will be straightforwardly interpretable (applications of network theory in brain imaging contexts can present interpretational challenges as the graphs tend to consist of non-directed, temporally static snapshots of nodal connections) and we expect, would produce both interesting immediate results and also intriguing new questions.

4. *Data*. This framework easily accommodates measurements of all types taken simultaneously on the same windowed time intervals, allowing potentially powerful integration of multiple modalities [23] and multiple time-varying features taken from the same imaging modality: the relationships between characteristic states drawn from any imaging modality or measurement at time $t + 1$ can condition, or fail to condition on characteristic states of any other at time t. Extending the kind of analysis introduced here into multiple modalities (e.g.,

simultaneous fMRI-EEG) or types of measurement (windowed spectral measurements from fMRI and windowed network connectivity from fMRI) seems a promising direction for future research. Also, incorporating task data as an augmentation to resting state for the same set of subjects might expose important informational roles for JFDCs that appear shy or even insular under resting conditions.

5. *Statistical Robustness and Null Models*. This is a multilayered approach with many stages where choices are made upon which results will be dependent to some degree. A clearer understanding of the ways in which results are sensitive to choices made in early processing stages will be important in applications. The null model for significance of the information flow metric can also be refined in ways that would allow for more interesting interpretation of the information flow results.

V. Conclusion

We have introduced an intuitive, flexible and highly extensible new method of investigating brain connectivity that captures information flow and directional patterns of organizational influence at the scale of broad functionally integrated domains. This method has allowed us to identify domain-pairs whose time-varying connectivity structures play distinguished roles in shaping functional relationships throughout the brain, so-called *global catalyzers*. We have also found, conversely, that temporal changes in intra-domain connectivity between auditory, visual and sensorimotor networks (AVSNs) – a set of networks that tend to be highly inter-correlated even under eyes-closed resting conditions – play a very limited role in organizing behavior in the remainder of the resting brain, including behavior that involves AVSN connections to other functional domains. The degree of sensitivity that intra-AVSN connectivity exhibits to broader functional brain interactions depends on subject clinical status: in healthy subjects, intra-AVSN connectivity patterns respond are responsive to variations exhibited the relationships of networks in other domain-pairs; in schizophrenia intra-AVSN connectivity is *insular*, it neither influences nor responds to changes in network relationships in domain-pairs in which at least one constituent functional domain is non-AVSN. Intra-cerebellar connectivity (CR-CR, a joint domain consisting of only two networks) was shown to be responsive to input but non-influential (a *shy* joint domain) but for CR-CR this property did not vary by subject clinical status. The ability to characterize functional domains in terms of both their role in shaping overall time-varying functional brain relationships and also their degree of responsiveness to the ambient time-varying connectivity environment is a distinctive feature of the method introduced here. We believe that, in combination with joint-domain-specific representations of dynamic connectivity, it significantly augments the information landscape on which complex brain disorders and associated cognitive/behavioral abnormalities can be studied.

Acknowledgments

Research supported by NIH grants P20GM103472, R01EB005846, R01EB020407 and NSF 1539067.

References

1. Calhoun VD, Miller R, Pearlson G, Adali T. The Chronnectome: Time-Varying Connectivity Networks as the Next Frontier in fMRI Data Discovery. Neuron. Oct 22.2014 84:262–284. 2014. [PubMed: 25374354]
2. Hutchison RM, Womelsdorf T, Allen EA, Bandettini P, Calhoun VD, Corbetta M, et al. Dynamic functional connectivity: promises, issues, and interpretations. NeuroImage. 2013; 80:360–378. [PubMed: 23707587]
3. Friston KJ, Harrison L, Penny W. Dynamic Causal Modeling. Neuroimage. 2003; 19:1273–1302. [PubMed: 12948688]
4. Havlicek M, Friston KJ, Jan J, Brazdil M, Calhoun VD. Dynamic modeling of neuronal responses in fMRI using cubature Kalman filtering. NeuroImage. 2011; 56:2109–2128. [PubMed: 21396454]
5. Deshpande G, Hu X. Investigating Effective Brain Connectivity from fMRI Data: Past Findings and Current Issues with Reference to Granger Causality Analysis. Brain Connectivity. 2012; 2:235–245. [PubMed: 23016794]
6. Calhoun VD, Adali T. Multi-subject Independent Component Analysis of fMRI: A Decade of Intrinsic Networks, Default Mode, and Neurodiagnostic Discovery. IEEE Reviews in Biomedical Engineering. 2012; 5:60–73. [PubMed: 23231989]
7. Allen E, Damaraju E, Plis SM, Erhardt E, Eichele T, Calhoun VD. Tracking whole-brain connectivity dynamics in the resting state. Cereb Cortex. 2014; 24:663–676. [PubMed: 23146964]
8. Zalesky A, Fornito A, Cocchi L, Gollo LL, Breakspear M. Time-resolved resting-state brain networks. Proc Natl Acad Sci U S A. Jun 30.2014
9. Damaraju E, Allen EA, Belger A, Ford J, McEwen SC, Mathalon D, et al. Dynamic functional connectivity analysis reveals transient states of dysconnectivity in schizophrenia. Neuroimage: Clinical. 2014
10. Damaraju, E., Turner, J., Preda, A., Van Erp, T., Mathalon, D., Ford, JM., et al. American College of Neuropsychopharmacology. Hollywood, CA: 2012. Static and dynamic functional network connectivity during resting state in schizophrenia.
11. Bassett DS, Nelson BG, Mueller BA, Camchong J, Lim KO. Altered resting state complexity in schizophrenia. Neuroimage. Feb 1.2012 59:2196–2207. [PubMed: 22008374]
12. Fornito A, Zalesky A, Pantelis C, Bullmore ET. Schizophrenia, neuroimaging and connectomics. Neuroimage. Oct 1.2012 62:2296–2314. [PubMed: 22387165]
13. Lynall ME, Bassett DS, Kerwin R, McKenna PJ, Kitzbichler M, Muller U, et al. Functional Connectivity and Brain Networks in Schizophrenia. Journal of Neuroscience. Jul 14.2010 30:9477–9487. [PubMed: 20631176]
14. Miller, RL., Yaesoubi, M., Calhoun, VD. Presented at the EMBC. Chicago, IL: 2014. Higher Dimensional Analysis Shows Reduced Dynamism of Time-Varying Network Connectivity in Schizophrenia Patients.
15. Pettersson-Yeo W, Allen P, Benetti S, McGuire P, Mechelli A. Dysconnectivity in schizophrenia: Where are we now? Neuroscience and Biobehavioral Reviews. Apr.2011 35:1110–1124. [PubMed: 21115039]
16. Rashid, B., Damaraju, E., Calhoun, VD. Proc HBM. Seattle, WA: 2013. Comparison of resting state dynamics in healthy, schizophrenia and bipolar disease.
17. Miller RL, Yaesoubi M, Turner J, Mathalon D, Preda A, Pearlson G, et al. Higher Dimensional Meta-State Analysis Reveals Reduced Resting fMRI Connectivity Dynamism in Schizophrenia Patients. PLoS ONE. in press.
18. Calhoun VD, Sui J, Kiehl KA, Turner JA, Allen EA, Pearlson GD. Exploring the Psychosis Functional Connectome: Aberrant Intrinsic Networks in Schizophrenia and Bipolar Disorder. Frontiers in Neuropsychiatric Imaging and Stimulation. 2012; 2:1–13.
19. van den Heuvel MP, Fornito A. Brain Networks in Schizophrenia. Neuropsychology Review. Mar. 2014 24:32–48. [PubMed: 24500505]
20. Venkataraman A, Whitford TJ, Westin CF, Golland P, Kubicki M. Whole brain resting state functional connectivity abnormalities in schizophrenia. Schizophrenia Research. Aug.2012 139:7–12. [PubMed: 22633528]

21. Gopal S, Miller RL, Michael A, Adali T, Cetin M, Rachakonda S, et al. Spatial Variance in Resting fMRI Networks of Schizophrenia Patients: An Independent Vector Analysis. Schizophrenia Bulletin. Jan.2016 42:152–160. [PubMed: 26106217]

22. Insel T, Cuthbert B, Garvey M, Heinssen R, Pine DS, Quinn K, et al. Research Domain Criteria (RDoC): Toward a New Classification Framework for Research on Mental Disorders. American Journal of Psychiatry. Jul.2010 167:748–751. [PubMed: 20595427]

23. Calhoun VD, Sui J. Multimodal fusion of brain imaging data: A key to finding the missing link(s) in complex mental illness. Biological Psychiatry: Cognitive Neuroscience and Neuroimaging. in press.

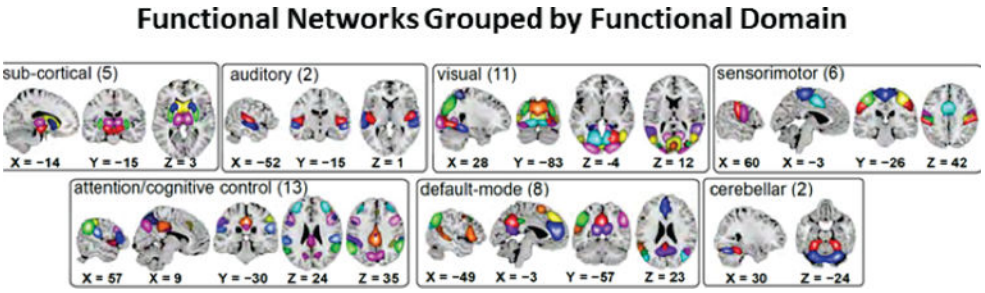

Fig. 1.

Composite maps displaying focal regions of resting state networks, grouped by functional domain [9];

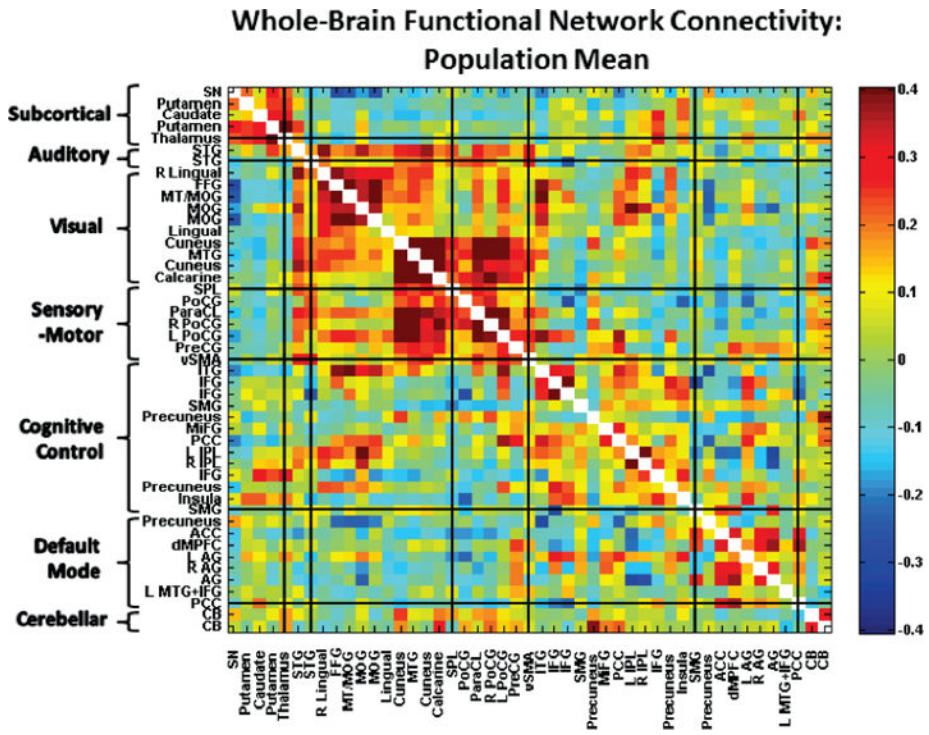

Fig. 2.

Population average of connectivity between networks, grouped along axes according to broad functional domain. Gridlines bound functional domains along each axis.

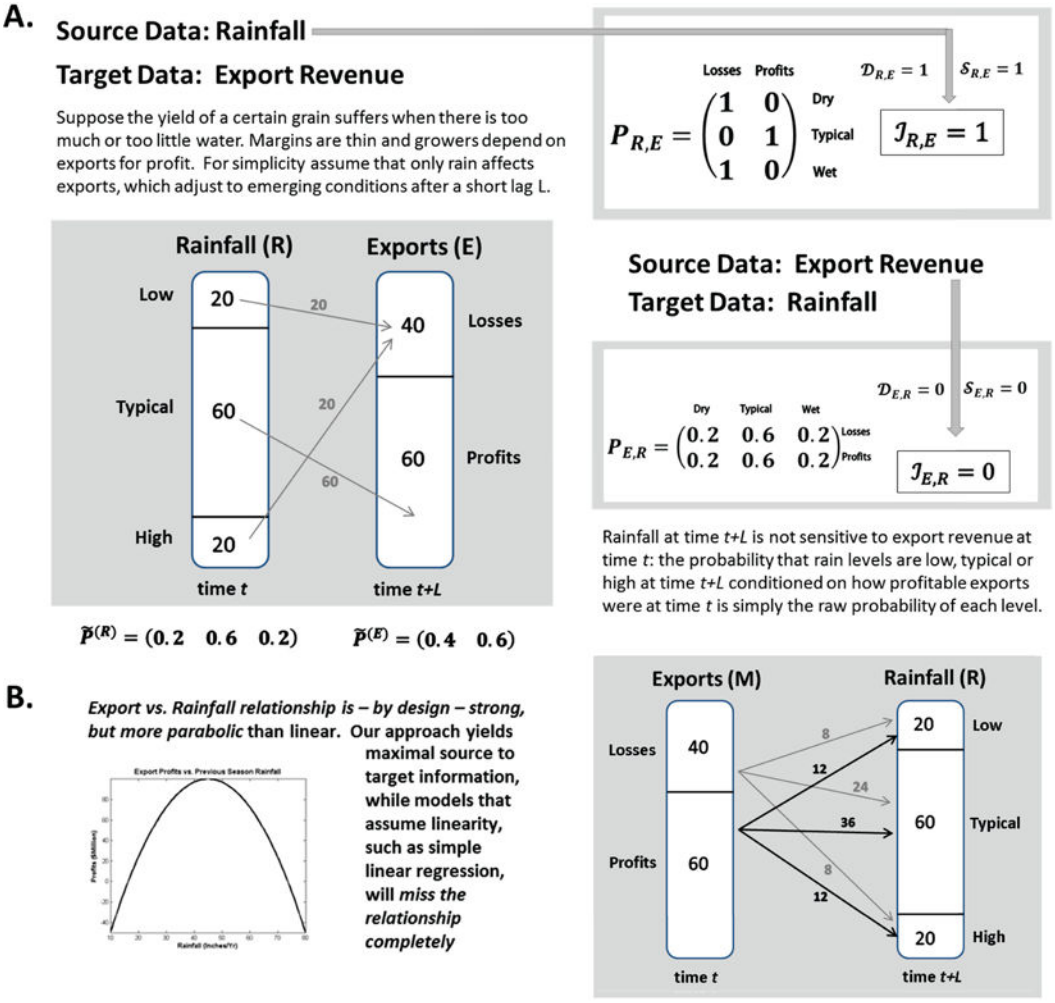

Fig. 3.

Stylized non-biological toy example of asymmetric intertemporal information flow between source and target data computed using the ddFDC methodology introduced here. In this example, there are 100 seasonal observations of rainfall and export revenues from a grain whose yield suffers when conditions are either too dry or too wet. The grain is stored for a period prior to export, so the effect of rainfall on export revenue is lagged. We make many simplifying assumptions to increase the clarity of the example: i.e, grain exports are only affected by rainfall, margins are very narrow so growers profit only when rainfall is in a fixed range, etc. Formal definitions of $\mathscr{D}$, $\mathscr{S}$ and $\mathscr{J}$ can be found in II.E. (A, top left) Forward time mapping from rainfall clusters to export revenue clusters; (A, top right) $\boldsymbol{P}_{\boldsymbol{R},\boldsymbol{E}}$ computed directly from (A, top left); the clusters of rainfall distribute as differently as possible over the clusters of grain revenue ($\mathscr{D}_{\mathrm{R,E}}=1$) and each rainfall cluster maps with maximal specificity to some cluster in export revenue ($\mathscr{S}_{\mathrm{R,E}}=1$). Thus, the intertemporal information $\mathscr{J}_{\mathrm{R,E}}=\frac{1}{2}(\mathscr{D}_{\mathrm{R,E}}+\mathscr{S}_{\mathrm{R,E}})$ from rainfall to grain export revenue is as large as possible: $\mathscr{J}_{\mathrm{R,E}}=1$. (A, bottom right) On the other hand, the same computation done from

export revenue to rainfall yields $\mathcal{J}_{\mathrm{E,R}}=0$. Rainfall is indifferent to the previous season's export revenue. The clusters of export revenue distribute identically in forward time over the clusters of rainfall, and none maps more preferentially to a given rainfall target than would be expected based on the raw distribution of rainfall data. (B) The conditional relationship of export revenue on the previous season's rainfall is designed to have a positive max for typical rainfall levels, and to be negative whenever rainfall is below/above fixed thresholds. The relationship is very strong and captured easily with our method while methods assuming a specific functional form, certainly those assuming a linear relationship would miss it completely.

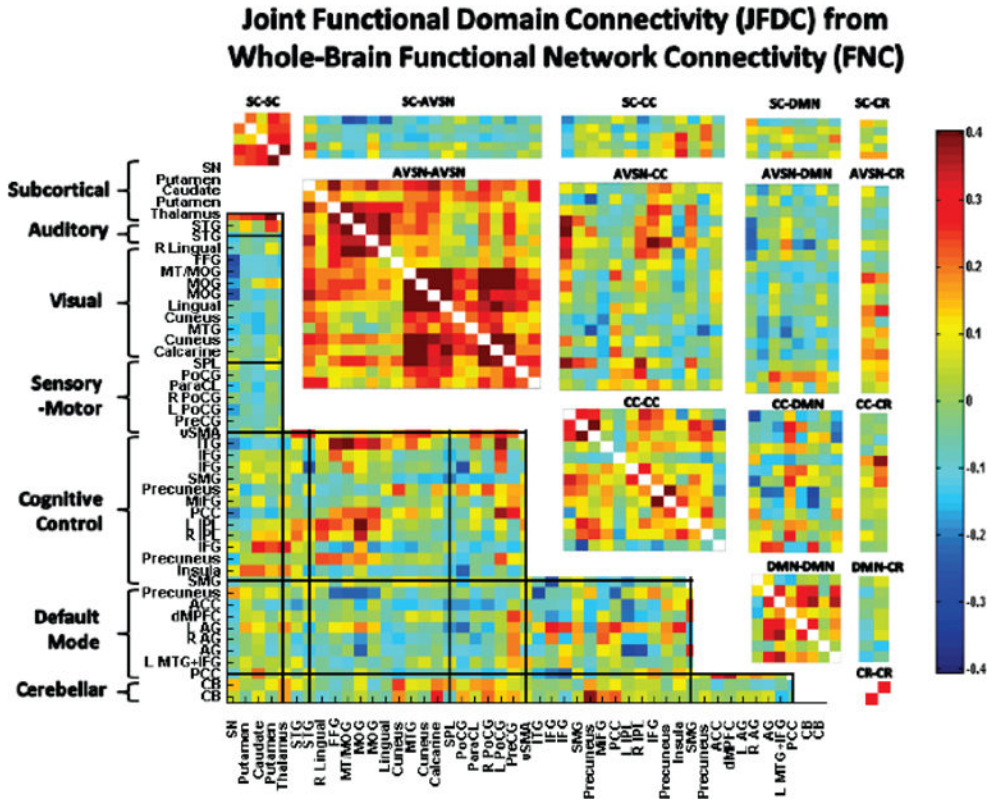

Fig. 4.

Population average of static whole-brain functional network connectivity, i.e., using all 162 timepoints (no windowing) for all 47 functional networks obtained from a GICA decomposition of our data. Grid lines bound the original 7 functional domains identified in earlier treatments of functional network connectivity in this dataset [9]. Rectangular pull-outs are the 15 JFDCs arising from the reduced set of 5 functional domains employed here (in this study, to modestly reduce overall dimensionality of the analysis, we combined the highly interconnected auditory, visual and sensorimotor networks into one larger auditory-visual-sensorimotor (AVSN) domain.

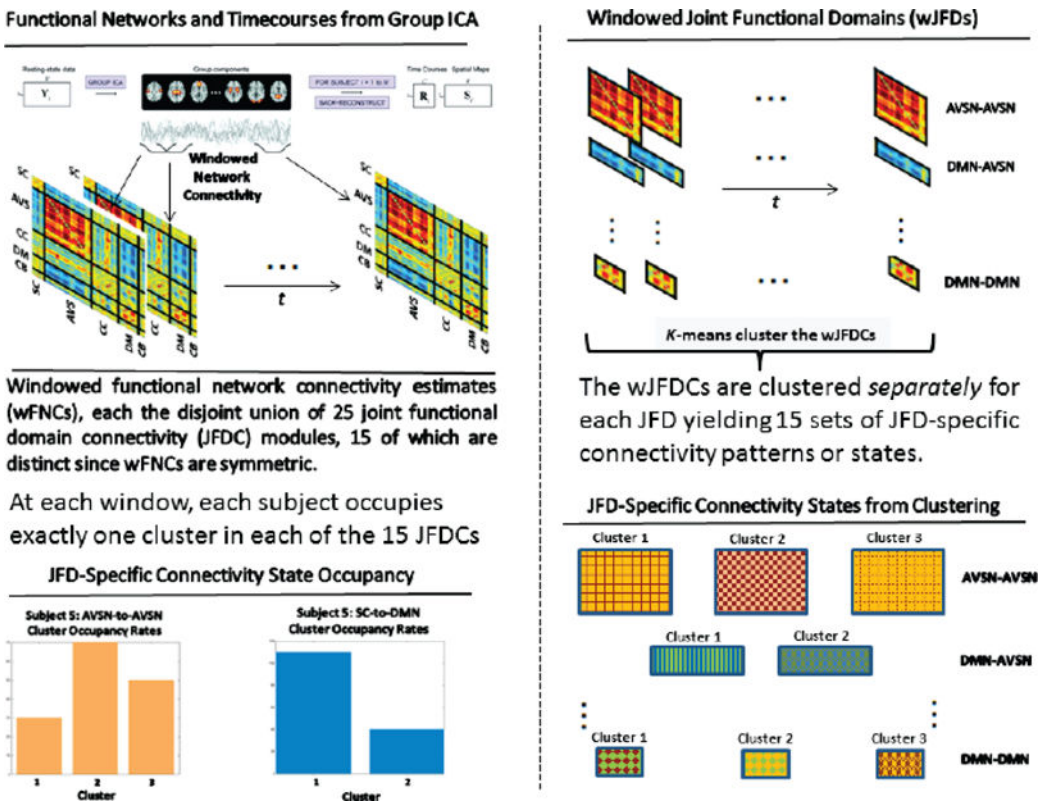

Fig. 5.

Schematic illustration of early-stage processing of our data from fMRI scans to windowed FNC estimates (top left); to windowed JFDCs (top right), to JFD-specific dynamic connectivity “states” summarizing recurring patterns of connectivity between networks in the corrsponding JFDs (bottom right); to information about subjects’ time-varying connectivity at a JFD-specific level of resolution.

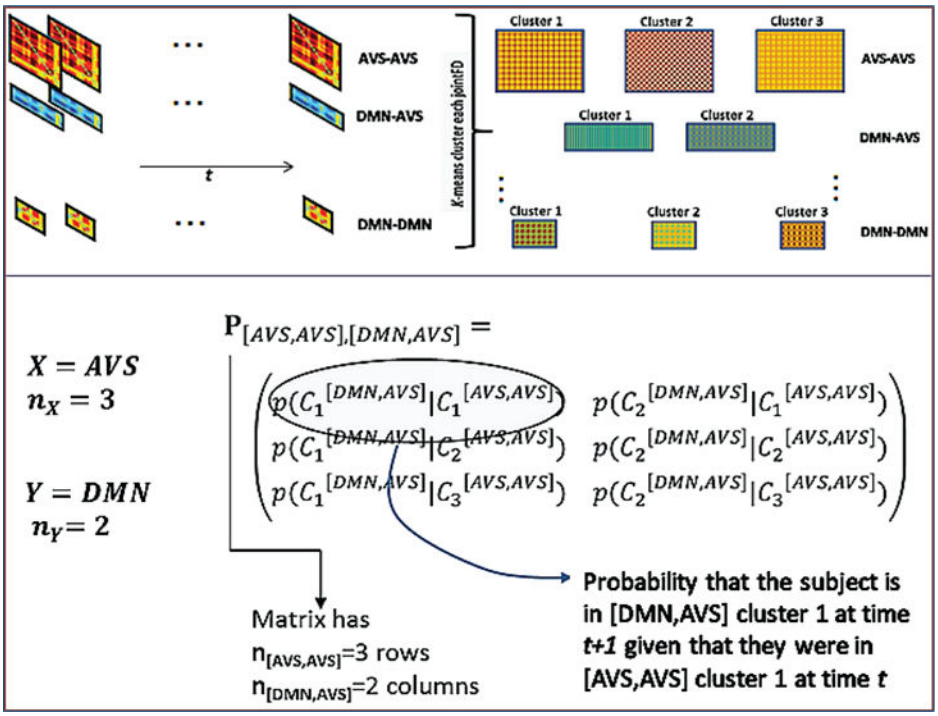

Fig. 6.

Schematic illustration of how intertemporal cross-JFDC probability transition matrices are produced, starting with the extraction of dynamic JFD-specific connectivity states from windowed JFDCs (top); to computation of the probability, for a given pair of JFDs, that each target cluster is realized at time ***t*** + **1** given occupancy of each source cluster at time ***t*** (bottom).

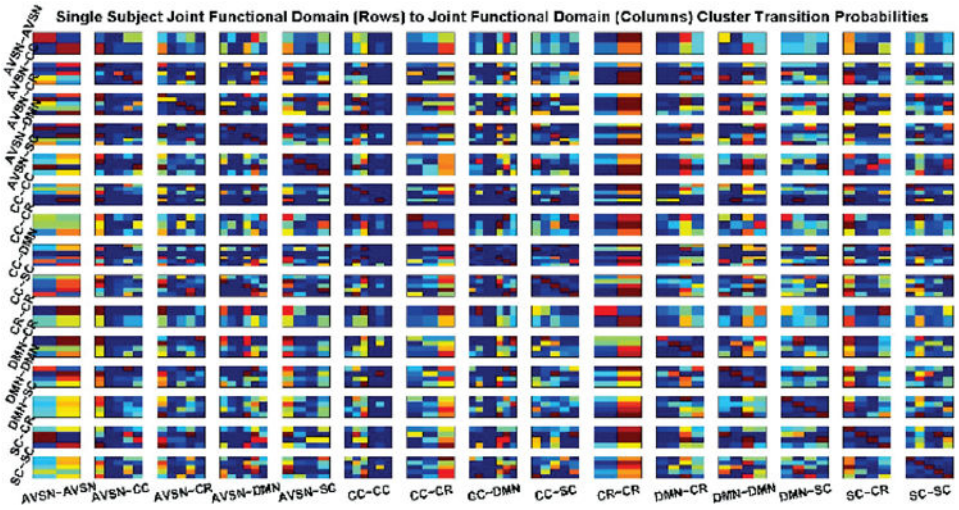

Fig. 7.

Array exhibiting one subject's (56 y.o. female schizophrenia patient) cross-JFDC transition probabilities matrices. The rows of the array are labeled by source JFDs. The columns of the array are labeled by target JFDs. The colormap is normalized on columns of the array, i.e., over target JFDs.

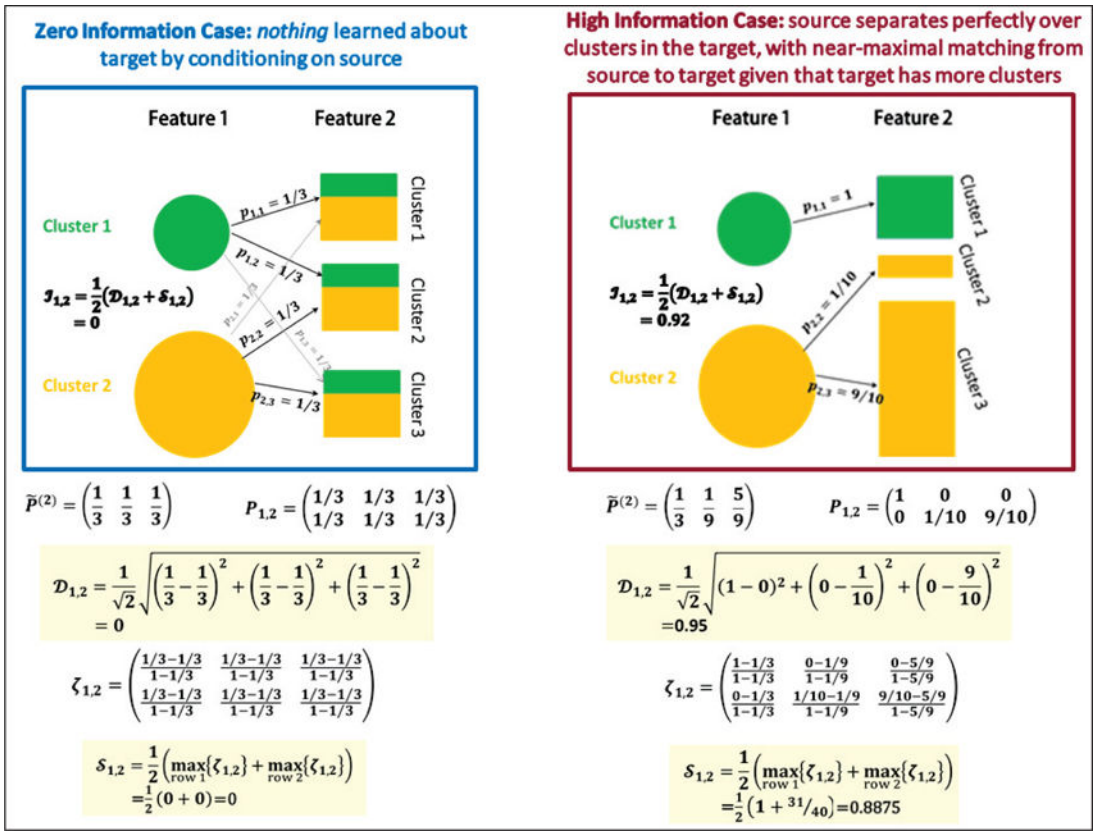

Fig. 8.

Information flow from a source with two clusters (at time ***t***) to a target with three clusters (at time ***t*** + **1**). In the zero-information case (left) occupancy of target clusters is independent of source cluster identity at the preceding timestep. Here, the source cluster structure provides no information about subsequent properties of the target feature: $\mathcal{D}_{1,2}=0$ and $\mathcal{S}_{1,2}=0$, so $\mathcal{J}_{1,2}=0$. In a high-information case (right) the occupancy rate of target clusters depends heavily on source cluster identity at the immediately preceding timestep. Each of the two source clusters distributes differently over the target clusters ($\mathcal{D}_{1,2}=0.95$) and each source cluster maps with very high probability to a particular target cluster ($\mathcal{S}_{1,2}=0.8875$), inducing a high overall measure ($\mathcal{J}_{1,2}=0.92$) of intertemporal information flow from source to target.

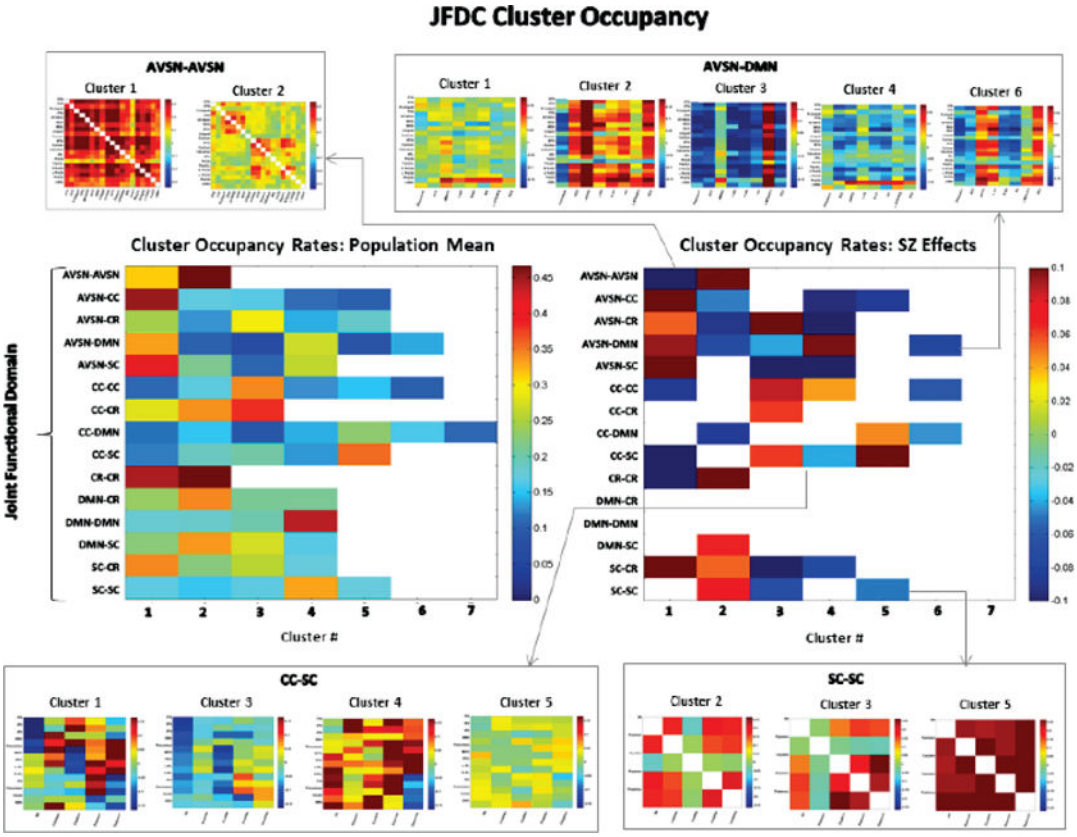

Fig. 9.

(A) Mean occupancy rates of clusters in each JFDC; (B) Significant (FDR-corrected at α = 0.05 level) SZ effects (red is positive correlation with SZ; blue is negative correlation with SZ) on cluster occupancy rates. With the exception of DMN-CR and DMN-DMN, a large proportion of clusters in most JFDCs are significantly affected by diagnosis. Actual centroids of clusters in four JFDCs (AVSN-AVSN, AVSN-DMN, CC-SC and SC-SC) whose occupancy rates are significantly affected by SZ diagnosis are displayed in boxes, with arrows from the row containing relevant occupancy rate diagnosis effects. In three of the four displayed JFDCs, we see at least one under-connected (low magnitude connectivity between many constituent network pairs) cluster centroid with significantly higher occupancy among patients (AVSN-AVSN, Cluster 2; AVSN-DMN, Cluster 1; CC-SC, Cluster 5). This is consistent with previous findings of diminished whole-brain functional network connectivity in SZ patients from both static and dynamic FNC studies. There are also novel characteristics of time-varying connectivity evidenced even in the handful of JFDC cluster centroids displayed above: AVSN-DMN, Cluster 2 exhibiting strong positive connections between AVSNs and most DMN networks is not seen either in the static FNC from this data (Fig. 4) or among the whole-brain dynamic connectivity states reported in an earlier study [9] that were obtained from clustering the whole-brain wFNCs from which our wJFDCs were drawn; CC-SC, Cluster 3 with many strong positive connections between CC and SC networks is another recurring pattern of cross-JFDC connectivity that is neither evident in static FNC nor in the dynamic connectivity states from [9].

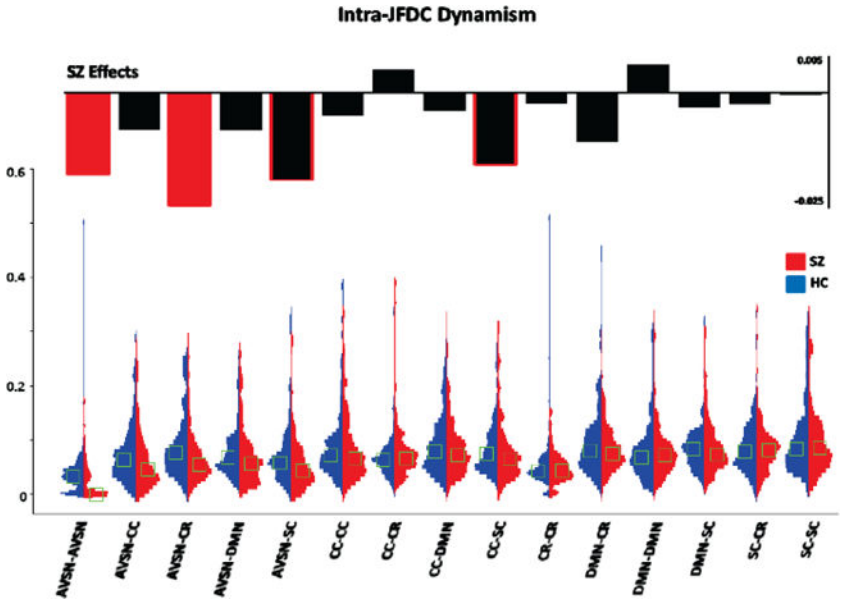

Fig. 10.

(Bottom) The distributions (HC blue, SZ red, medians marked with green boxes) of the intra-JFDC dynamism measure $\boldsymbol{d_i}$; (Top) Schizophrenia regression effects on $\boldsymbol{d_i}$ for each JFDC (bars outlined in red are significant at $\boldsymbol{\alpha}$ = 0.05 level, solid red bars survive FDR correction for multiple comparisons at this level). AVSN-AVSN and CR-CR have the lowest mean intra-JFDC dynamism. Schizophrenia most strongly suppresses intra-JFDC dynamism in AVSN-AVSN and AVSN-CR.

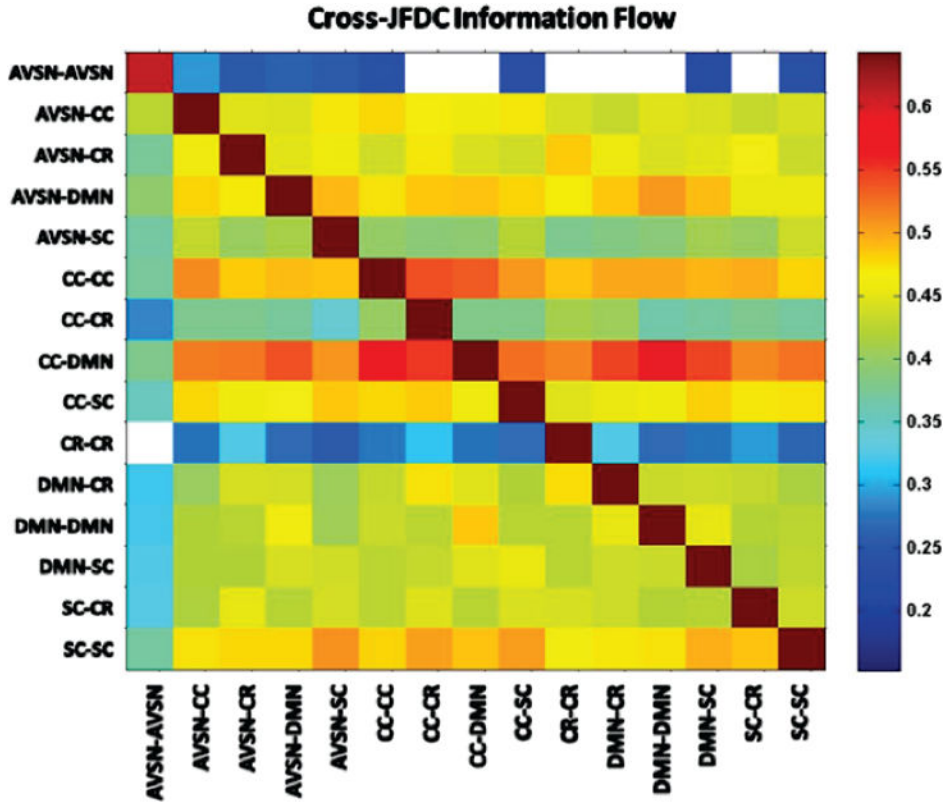

Fig. 11.

Population means of xJFDC (row JFDC *to* column JFDC) information flow $\mathcal{J}_{i,j}$, displayed where values exceed the 0.05-level null distribution significance threshold: most xJFDCs pass this threshold since much activation within the brain is temporally conditioned to some extent on other parts of the same brain on the $\boldsymbol{t}, \boldsymbol{t} + \mathbf{1}\boldsymbol{TR}$ timescale. Although some JFDCs have broad effects on connectivity throughout the brain, the sensitivity of JFDCs to connectivity between other functional units is generally more narrowly tuned: note that most columns feature a small number of isolated “hot spots”, while there is a rough uniformity of magnitude evident along certain rows Connectivity dynamics, for example, between networks involved with cognitive control (CC) and those in the default mode (DMN) play an unusually large role in shaping subsequent functional connectivity throughout the brain. Other JFDCs to which subsequent connectivity through much of the brain is highly sensitive include CC-CC, AVSN-DMN. SC-SC and CC-SC. Intra-domain connectivity between auditory-visual-sensorimotor networks (AVSN) and between cerebellar networks (CR), at least under eyes-closed resting conditions, show very little effect on subsequent connectivity even in the JFDCs in which they are a constituent FD. There is directional asymmetry in evidence here, with AVSN-AVSN connectivity conditioning somewhat less weakly on input from other JFDCs than the other way around, and intra-cerebellar connectivity much more sensitive to broader brain connectivity patterns than it is influential.

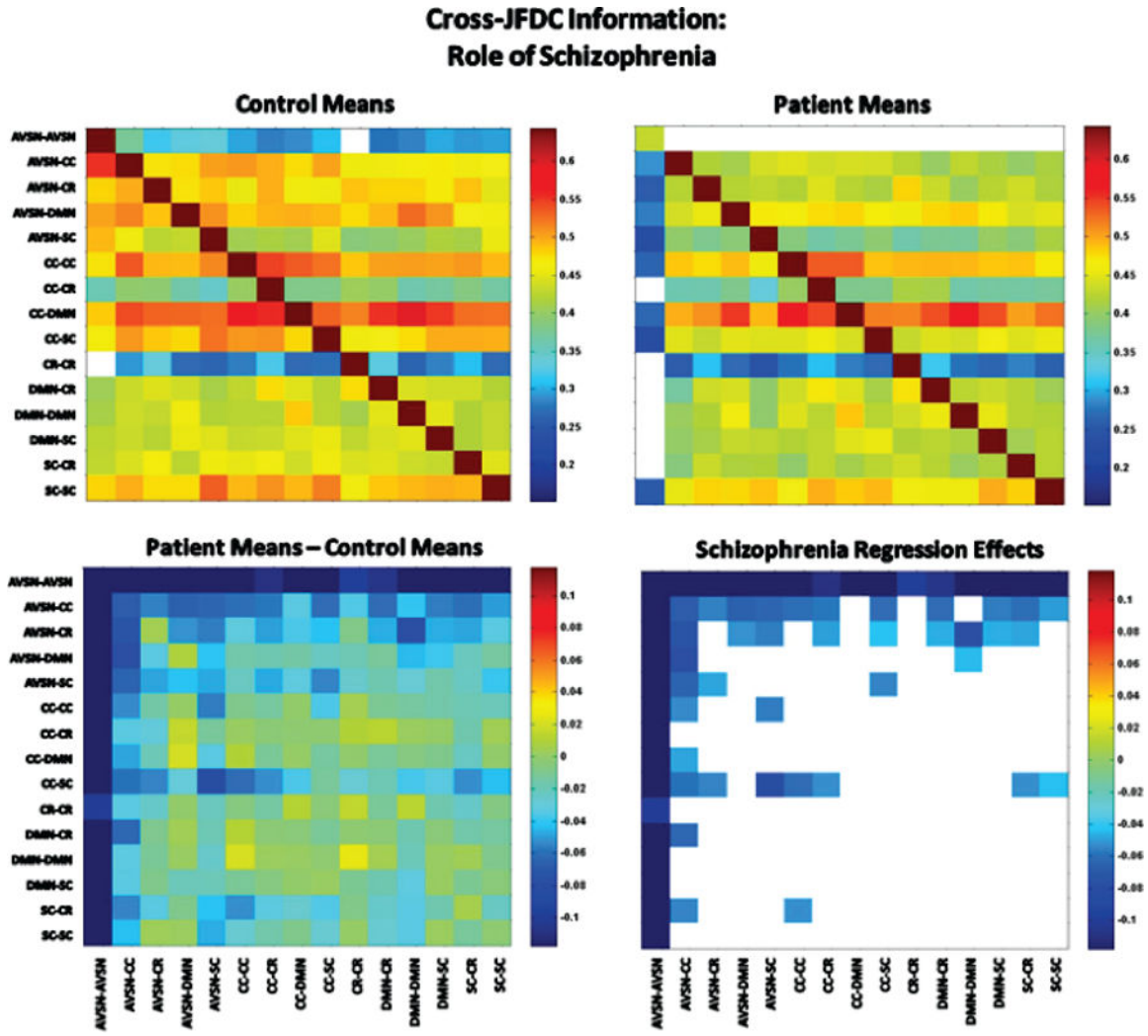

Fig. 12.

Schizophrenia exerts highly significant negative effects on xJFDC intertemporal information flow, applying particularly to AVSN-AVSN and to information outflow from AVSN-CC and CC-SC. The sensitivity of intra-AVSN connectivity to inputs from broader brain connectivity patterns is much higher in healthy individuals, actually rendering this JFDC non-insular in the healthy population. Negative SZ effects falling slightly below the FDR cutoff for significance at the **0.05**-level apply to information flow both into and out of AVSN-SC, and for information flow into DMN-DMN. Displayed patient and control means have been corrected for confounding effects of age and gender. Only regression effects that survive FDR correction for multiple comparisons at **0.05**-level are displayed.

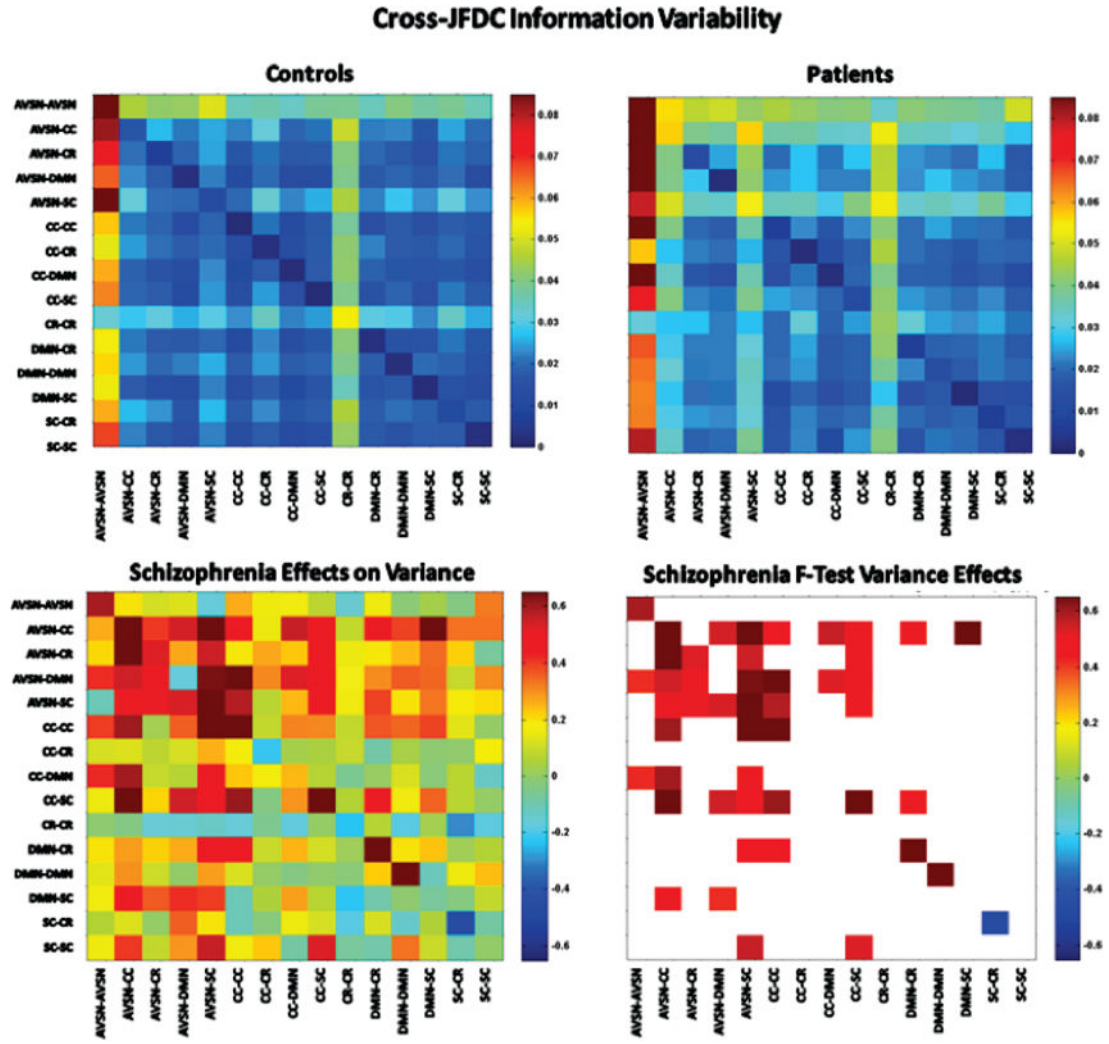

Fig. 13.

Cross-JFDC information flow into AVSN-AVSN exhibits the highest inter-subject variability in both patients and controls. Patient variability in information both into and out of AVSN-SC and involving AVSN-CC is somewhat higher than other xJFDCs. Patients, as a group, exhibited significantly more variability in xJFDC information flow than did controls (F-statistic displayed for FDR-corrected $\boldsymbol{\alpha}$ = **0.05** significance level).

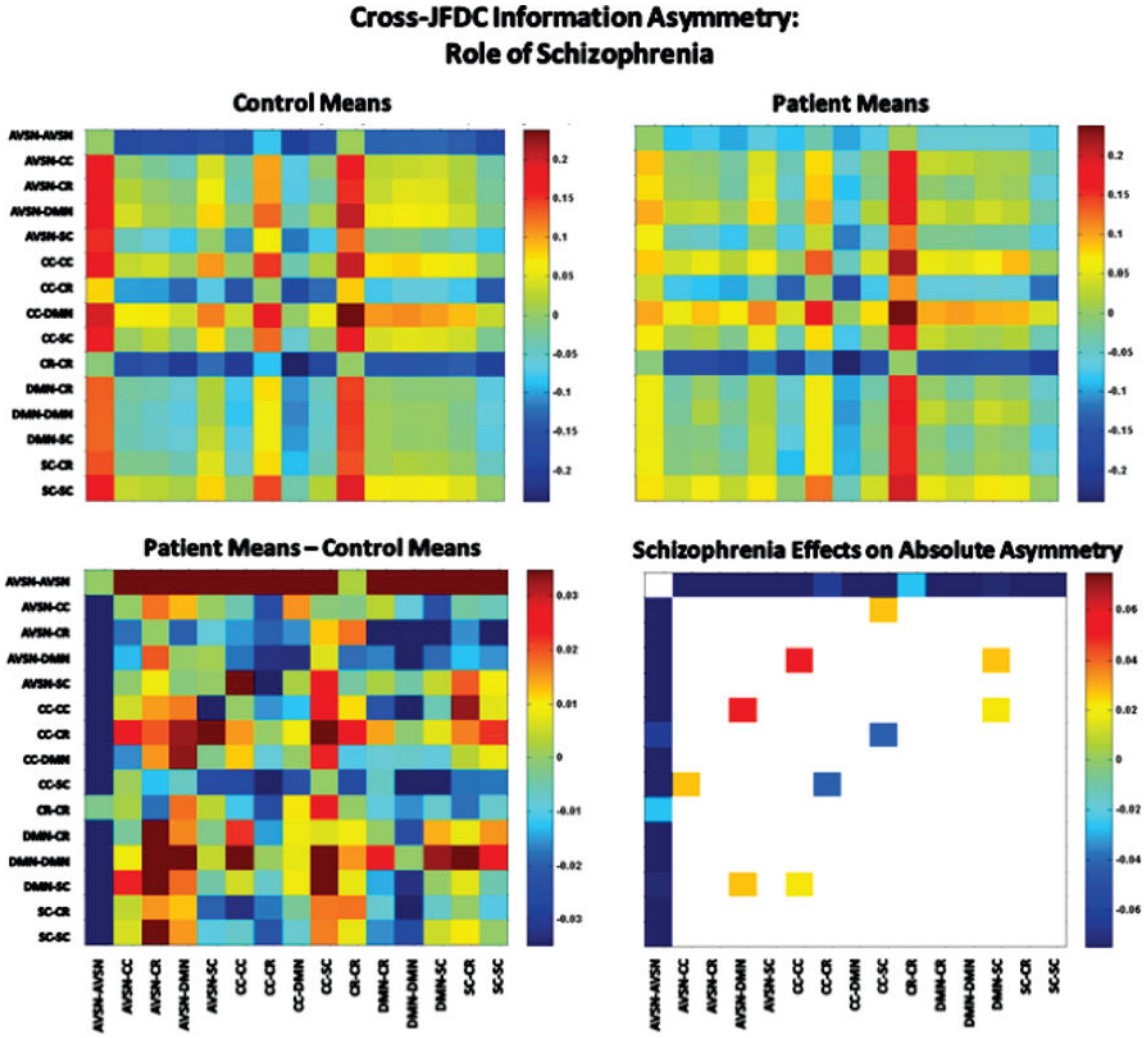

Fig. 14.

The direction of the higher-magnitude signed information flow asymmetries (top row) is relatively stable between patients and controls, but strength is often more pronounced in controls. Inflow of information from other JFDCs to AVSN-AVSN strongly exceeds outflow in controls, while this imbalance is weaker in patients. This observation also applies to several JFDCs with a cerebellar component. Among the JFDCs that show evidence of information asymmetry going the other direction: more information outflow to other JFDs than inflow from other functional units are CC-CC, CC-DMN and SC-SC.

Table 1

The average number of clusters realized per subject in each JFDC, plus the aggregate realization rate (final column). Patient and control group means, and schizophrenia regression effects on realization rates with corresponding p-values are also reported. The SZ effect is significant at the **0.05**-level following FDR correction (***p*** < **0.012**) for all AVSN-related JFDCs as well as CC-CC.

JFDC Clusters Realized Per-Subject								
JFDC	**AVSN-AVSN**	**AVSN-CC**	**AVSN-CR**	**AVSN-DMN**	**AVSN-SC**	**CC-CC**	**CC-CR**	**CC-DMN**
#of Clusters	***2***	***5***	***5***	***6***	***4***	***6***	***3***	***7***
Avg/Sub (Pop)	1.67	3.44	3.70	3.98	2.90	4.46	2.82	5.04
Avg/Sub (SZ)	1.47	3.07	3.48	3.78	2.65	4.29	2.84	4.93
Avg/Sub (HC)	1.85	3.77	3.91	4.17	3.13	4.61	2.80	5.15
SZ Effect	*−0.38*	*−0.69*	*−0.43*	*−0.38*	*−0.47*	*−0.30*	0.04	−0.22
Pval	0.00	0.00	0.00	0.00	0.00	0.01	0.33	0.09
JFDC	**CC-SC**	**CR-CR**	**DMN-CR**	**DMN-DMN**	**DMN-SC**	**SC-CR**	**SC-SC**	***TOTAL***
#of Clusters	***5***	***2***	***4***	***4***	***4***	***4***	***5***	***66***
Avg/Sub (Pop)	3.92	1.94	3.60	3.39	3.63	3.51	4.16	**52.16**
Avg/Sub (SZ)	3.70	1.95	3.58	3.42	3.59	3.49	4.13	**50.36**
Avg/Sub (HC)	4.13	1.93	3.62	3.37	3.67	3.52	4.18	**53.86**
SZ Effect	−0.42	0.01	−0.04	0.04	−0.08	−0.03	−0.04	***−3.39***
Pval	0.00	0.67	0.55	0.58	0.18	0.73	0.67	**0.00**